Supplement 1: Deriving a predator's spatial invasion fitness.

For the spatial model described in the main text, the spatial moment equations are as follows.

$$\begin{aligned}\frac{dP_{PO}}{dt} &= (d+\alpha\cdot(1-e)\cdot\theta)\cdot P_{NP}+\alpha\cdot(1-\theta)\cdot q_{P|NO}\cdot P_{NO}\\ &+(m+\alpha\cdot(1-e)\cdot(1-\theta)\cdot q_{N|PP})\cdot P_{PP}\\ &-(m+\alpha\cdot(1-e)\cdot(1-\theta)\cdot q_{N|PO}+r\cdot(1-\theta)\cdot q_{N|OP})\cdot P_{PO}\\ &+m_P\cdot(1-\theta)\cdot(q_{P|OO}\cdot P_{OO}-q_{O|PO}\cdot P_{PO}+q_{O|PP}\cdot P_{PP}-q_{P|OP}\cdot P_{PO})\end{aligned} \tag{S.1}$$

$$\begin{aligned}\frac{dP_{PN}}{dt} &= r\cdot(1-\theta)\cdot q_{N|OP}\cdot P_{OP}+\alpha\cdot(1-\theta)\cdot q_{P|NN}\cdot P_{NN}\\ &-(m+d+\alpha\cdot(\theta+(1-\theta)\cdot q_{P|NP})+\alpha\cdot(1-e)\cdot(1-\theta)\cdot q_{N|PN})\cdot P_{NP}\\ &+m_P\cdot(1-\theta)\cdot(q_{P|ON}\cdot P_{NO}-q_{O|PN}\cdot P_{PN})\end{aligned} \tag{S.2}$$

$$\begin{aligned}\frac{dP_{PP}}{dt} &= 2\cdot\alpha\cdot(e\cdot\theta+(1-\theta)\cdot q_{P|NP})\cdot P_{NP}-2\cdot m\cdot P_{PP}\\ &-2\cdot(\alpha\cdot(1-e)\cdot(1-\theta)\cdot q_{N|PP}+m_P\cdot(1-\theta)\cdot q_{O|PP})\cdot P_{PP}\\ &+2\cdot m_P\cdot(1-\theta)\cdot q_{P|OP}\cdot P_{OP}\end{aligned} \tag{S.3}$$

$$\begin{aligned}\frac{dP_{NO}}{dt} &= (m+\alpha\cdot(1-e)\cdot(1-\theta)\cdot q_{N|PN})\cdot P_{NP}+d\cdot P_{NN}\\ &+r\cdot(1-\theta)\cdot q_{N|OO}\cdot P_{OO}\\ &-(d\cdot+\alpha\cdot(1-\theta)\cdot q_{P|NO}+r\cdot\theta+r\cdot(1-\theta)\cdot q_{N|ON})\cdot P_{NO}\\ &-m_P\cdot(1-\theta)\cdot(q_{P|ON}\cdot P_{NO}+q_{O|PN}\cdot P_{PN})\end{aligned} \tag{S.4}$$

$$\begin{aligned}\frac{dP_{OO}}{dt} &= 2\cdot d\cdot P_{NO}+2\cdot(m+\alpha\cdot(1-e)\cdot(1-\theta)\cdot q_{N|PO})\cdot P_{PO}\\ &-2\cdot(r\cdot(1-\theta)\cdot q_{N|OO}+m_P\cdot(1-\theta)\cdot q_{P|OO})\cdot P_{OO}\\ &+2\cdot m_P\cdot(1-\theta)\cdot q_{O|PO}\cdot P_{PO}\end{aligned} \tag{S.5}$$

$$\frac{dP_{NN}}{dt} = 2\cdot r\cdot(\theta+(1-\theta)\cdot q_{N|ON})\cdot P_{NO}-2\cdot(d-\alpha\cdot(1-\theta)\cdot q_{P|NN})\cdot P_{NN} \tag{S.6}$$

where P_{XY} is the density of XY pairs on the lattice (N is a site occupied by a prey individual, P is a site occupied by a predator individual, and O is an empty site) and $q_{X|YZ}$ is the average density of X next to Y with a Z neighbor on the lattice. P_{XY} is equal to P_{YX} but $q_{X|YZ}$ is not equal to $q_{X|ZY}$.

In particular, $q_{X|YZ}$ is equal to P_{XYZ}/P_{YZ} while $q_{X|ZY}$ is equal to P_{XZY}/P_{ZY}. While the denominators of the two expressions are equivalent, the density of *XYZ* triplets is not necessarily equal to the density of *XZY* triplets. In addition, because the *q* terms are functions of pair and triplet densities, they are dynamic and change through time in concordance with the change in pair densities.

The dynamics of the predator on the lattice is the sum of equations S.1-3. Since $q_{X|YZ}*P_{YZ} = P_{XYZ}$ and, for example, $P_{NPP} + P_{NPN} + P_{NPO}=P_{NP}$, the sum simplifies to

$$\frac{dP_P}{dt} = \alpha \cdot e \cdot q_{N|P} \cdot P_P - m \cdot P_P \tag{S.7}$$

Note that the movement rate, m_P, does not enter directly into this equation. The equilibrium value of $q_{N|P}$ can be obtained from eq. S.7.

$$\hat{q}_{N|P} = \frac{m}{\alpha \cdot e} \tag{S.8}$$

Given equation S.7, and assuming that the invader quickly affects is local environment without changing the global environment (reaching a quasi-equilibrium state), the invasion fitness of a predator is

$$\frac{1}{P_P} \cdot \frac{dP_P}{dt} = \alpha \cdot e \cdot \hat{q}^o_{N|P} - m \tag{S.9}$$

Rearranging, and substituting with eq. S.8 gives

$$\frac{1}{P_P} \cdot \frac{dP_P}{dt} = \alpha \cdot e \cdot (\hat{q}^o_{N|P} - \hat{q}_{N|P}) \tag{S.10}$$

This equation (shown in the main text) is in a different form than has appeared in other publications in the context of pathogen-host interactions [1]. Specifically, we assume only local interactions, with no possibility for random interactions. This simplifies the criterion for invasion success such that the resident predator's equilibria do not contribute. In addition, we replace the quantity $m/\alpha e$ that appears in transitioning from S.9 to S.10 with $\hat{q}_{N|P}$. This allows a more

intuitive understanding of the invasion criterion in the context of R^* theory as presented in the main text.

Supplement 2: Non-spatial predator prey model and evolutionary predictions.

In the absence of spatial structure, the population dynamics of a predator and its prey can be described by the following equations.

$$\frac{dN}{dt} = (r - d) \cdot N - \alpha \cdot N \cdot P \quad \text{(S.12)}$$

$$\frac{dP}{dt} = \alpha \cdot e \cdot N \cdot P - m \cdot P \quad \text{(S.13)}$$

In these equations, N is the prey population size, P is the predator population size, r is the prey reproduction rate, d is the prey death rate, α is the predator attack rate, e is the prey-to-predator conversion efficiency (the ratio of predators produced per prey eaten), and m is the predator death rate. If the conversion efficiency is 1 and the predator death rate is an additive function of the prey death rate (i.e. $m=d+c$ where c is some positive constant such that $d/m<1$), these equations are structurally identical to a susceptible-infected model of pathogen-host interactions where the prey is the susceptible host population and the predator is the infected host population.

An invasion analysis using the L-V model of predator prey interactions (equations S.12 and S.13) yields the following. A predator's per-capita population growth rate is

$$\frac{1}{P} \cdot \frac{dP}{dt} = \alpha \cdot e \cdot N - m \quad \text{(S.14)}$$

When the predator is invading a prey population already at equilibrium with a resident predator, the per-capita population growth rate, and thus the predator's invasion fitness, is

$$\frac{1}{P_I} \cdot \frac{dP_I}{dt} = \alpha_I \cdot e_I \cdot N_R^* - m_I \quad \text{(S.15)}$$

where the subscripts *I* and *R* refer to the invading and resident predator (respectively) and N^* is the prey population size at equilibrium, given by

$$N_R^* = \frac{m_R}{\alpha_R \cdot e_R} \tag{S.16}$$

Thus, a predator can invade a prey population at equilibrium with a resident predator when

$$\alpha_I \cdot e_I \cdot \left(\frac{m_R}{\alpha_R \cdot e_R} - \frac{m_I}{\alpha_I \cdot e_I} \right) > 0 \tag{S.17}$$

In other words, when the invader's equilibrium prey population size is less than the resident's equilibrium prey population size, the invasion will succeed. Because the equilibrium prey population size is inversely related to the predator attack rate, a predator with a higher attack rate than the resident can always invade. Thus, the model predicts that evolution will lead to ever increasing predator attack rates. However, as the attack rate increases, the prey equilibrium population size decreases and becomes progressively more susceptible to extinction. If the prey goes extinct, the predator will follow. This prediction does not depend on the predator-prey traits that we show in the main text to influence the outcome of evolution in the spatial model, i.e. it holds regardless of the value of the prey reproduction rate, the ratio of prey and predator death rates, and the efficiency.

It is worth noting that certain assumptions about the ecology of the prey and predator, which are relevant to our spatial model, do not alter the evolutionary prediction outlined above. Of key importance to the invasion success of a predator is the prey equilibrium population size (eq. S.16). Mathematically, logistic prey growth (eq. S.18; inherent in our spatial model because the lattice is of a finite size) does not change the predicted prey equilibrium population size. Neither does prey growth limited by the predator population size (eq. S.19; inherent in our spatial model since prey cannot reproduce into sites occupied by predators). Thus, these

modifications are not mathematically predicted to impact the evolutionary outcome arising from the invasion analysis shown above. We have confirmed that the complexities of prey growth inherent in our spatial model do not alter the equilibrium prey population size predicted by eq. S.16 by running non-evolutionary spatial simulations with a predator and prey where interactions between lattice sites are random through time rather than locally structured in space. Thus, the equilibria of the simulation should match the equilibria from an equivalent non-spatial model. These simulations show that the prey equilibrium population size is indeed equal to S.16. Thus, the correct analogous non-spatial evolutionary prediction for our model can be arrived at by an invasion analysis of the simplest non-spatial model, given by eq's S.12 and S.13.

$$\frac{dN}{dt} = (r-d)\cdot N\cdot(1-\frac{N}{K}) - \alpha\cdot N\cdot P \tag{S.18}$$

$$\frac{dN}{dt} = (r-d)\cdot N\cdot(1-\frac{N}{K-P}) - \alpha\cdot N\cdot P \tag{S.19}$$

Supplement 3: Deriving the quasi-equilibrium density of prey around a predator.

The quasi-equilibrium $q_{N|P}$ for a predator invading a resident predator in equilibrium with the prey can be obtained by adding the invader to the system of equations S.1-6. In particular, the system would include four new equations for dP_IN/dt, dP_IO/dt, dP_IP_I/dt, and dP_IP/dt where the subscript I denotes the invading predator. Then, one can formulate equations for the rate of change in the $q_{X|Y}$ terms. In particular,

$$\frac{dq_{X|Y}}{dt} = \frac{d(P_{XY}/P_Y)}{dt} = \frac{1}{P_Y}\cdot\frac{dP_{XY}}{dt} - \frac{P_{XY}}{P_Y^2}\cdot\frac{dP_Y}{dt} \tag{S.11}$$

The invading predator's quasi-equilibrium can be obtained by solving the subset of equations S.11 where X or Y is P_I and setting all quantities that do not involve P_I to the equilibrium values for the resident predator (for example, $q_{O|N}$ would be set to the equilibrium value of $q_{O|N}$ for the system with only the resident predator). Since equations S.11 involve higher order correlations

(for example, dP_{PP}/dt depends on $q_{N|PP}$, the density of *NPP* triples divided by the density of *PP* pairs), one must use a moment closure approximation (for example, the ordinary moment closure approximation would make the simplifying assumption that $q_{N|PP} = q_{N|P}$).

Supplement 4: Parameter values.

Here we compare our model parameter values with the demographic rates estimated for real systems. This provides important perspective on the types of systems represented by our simulations.

Prey reproduction rate

The lowest prey reproduction rate used in our spatial simulations is 4 and the maximum is 50 (per prey generation). In the absence of the predator, the prey population is predicted to grow exponentially at a rate equal to *(r-d)* (called r_{max}) where *r* is the reproduction rate and *d* is the natural death rate. Thus, scaling time to be measured in prey generations (i.e. setting d=1), the minimum r_{max} in our model is 3/generation and the maximum is 49/generation. However, in the spatial model, the realized r_{max} is much lower because of the limited availability of empty sites for prey offspring to colonize. To determine the relationship between the realized r_{max} and the reproduction rate parameter *r*, we analyzed simulation data using a method often used to estimate r_{max} from observational data. In natural populations, r_{max} can be estimated by fitting population size data over time when the population starts from rarity with an exponential curve, where the exponent is r_{max}. We derive an equivalent “empirical" estimate from spatial simulation data by starting the simulation with no predator individuals and only one prey individual. This yields population size data over time starting from rarity, which can then be used to estimate r_{max}. We find that a reproduction rate of r=4/prey generation (r_{max}=3/prey generation) yields a realized r_{max} of ~0.5/prey generation and r=50/prey generation (r_{max}=49/prey generation) yields a realized

r_{max} of ~8/prey generation. The upper end of the range corresponds to arthropods (e.g. *Tribolium confusum* has an r_{max} of 8.5 [2]), while the lower end of the range corresponds to bacteria and protozoans (e.g. *Paramecium caudatum* has an r_{max}=0.28 [2]).

Prey conversion efficiency

We performed spatial simulations for prey conversion efficiencies of 0.2, 0.5 and 1. Empirical quantification of the prey conversion efficiency defined as the ratio of prey eaten to predator offspring produced is uncommon in the literature. More common are estimates of the energy conversion efficiency, or the proportion of prey mass consumed that is converted into predator body mass and used for individual predator growth. However, allometric scaling theory provides a framework within which the prey conversion efficiency can be estimated. It has been proposed that the prey conversion efficiency is proportional to the ratio of the prey to predator body size [3]. Using published body size data for a variety of predator and prey species [4] we calculated the mean prey to predator body size ratio for broad classes of predator and prey. This data does not provide exact prey conversion efficiencies but provides a relative understanding of how conversion efficiency varies between different types of predator-prey interactions.

Invertebrates eating invertebrates are at the upper end of the efficiency spectrum with an average body size ratio of 0.499 (based on body size in cm). Vertebrate predators of either vertebrate prey are in the middle range, with average body size ratios varying from 0.168 to 0.336 depending on the prey and predator metabolism (endotherm or ectotherm). Finally, vertebrate predators eating invertebrate prey are at the lower end of the efficiency specturm with an average body size ratio ranging from 0.035 to 0.045 depending on the metabolism of the prey.

Predator attack rate

The ES predator attack rate predicted by the spatial models used here range from 10 to 200 (per prey generation). The attack rate determines the per-capita prey consumption rate (number of prey consumed per predator per time). Specifically, at equilibrium the per-capita prey consumption rate is equal to the attack rate times the mean number of predator-prey interactions per predator. In a spatial context, the maximum number of predator-prey interactions per predator is 4 (since each lattice site has only 4 neighboring sites) and the minimum can be much less than 1. Thus, the minimum ES per-capita consumption rate predicted by the spatial model is nearly 0 and the maximum is 800 (per prey generation).

In the literature, the majority of estimates of per-capita consumption rates are for insect predators. For example, after 24 hours of starvation and with unlimited prey, *Cheilomenes sexmaculata* (a ladybug) can consume up to 200 *Aphis craecivora* (aphids) per day [5]. Assuming an aphid generation time of about 5.8 days [6], this is equivalent to a maximum per-capita consumption rate of over 1000 prey/predator/prey generation. A rare non-insect example, after 24 hours of starvation and with unlimited prey, *Cancer irroratus* (Atlantic rock crab) can consume 3 *Placopecten magellanicus* (Atlantic sea scallop) per day [7]. Assuming a scallop generation time of 5 years [8] yields a maximum per-capita consumption rate of 5,475 prey/predator /prey generation. In reality, the per-capita consumption rates of these organisms will likely be lower because of limited prey availability and predator satiation. However, these estimates give some perspective on the types of predators that represent the upper range of ES attack rates predicted by the spatial model. At the other end of the spectrum, a field study of *Crotalus viridis* (the Western rattlesnake) found that individual snakes consume about 6 prey items (including squirrels, rats, rabbits and mice) per year [9]. Assuming a rodent generation time of around 150 days [4] yields an attack rate of 2.5 prey/predator/prey generation.

Supplement 5: Measuring local prey density and cluster join rate.

To calculate the mean prey cluster size and cluster join rate, we first randomly choose a single, isolated prey individual at equilibrium in a non-evolutionary simulation of the predatory-prey dynamics. As the population dynamics proceed, we track the number of prey in the contiguous neighborhood of the chosen prey individual—a prey cluster. Because we use the Gillespie algorithm to simulate the dynamics, only one event occurs per small time interval. Thus, when a cluster grows by more than one prey individual, the event is counted as the joining of two prey clusters. Over the lifetime of the cluster we record its mean size and the number of join events. We collected data for at least 100 independent clusters for each parameter set. We then averaged the size and the number of joins per time across clusters.

Supplement 6: ES attack rate relative to extinction thresholds.

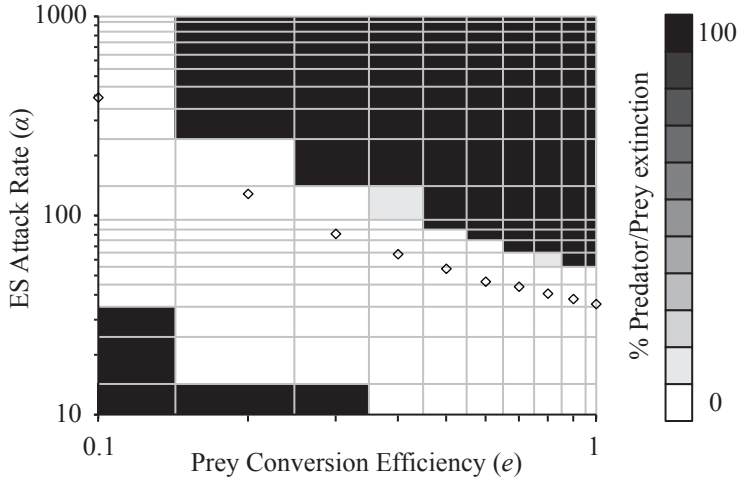

Figure S.1. ES attack rate relative to extinction thresholds. Data points are the ES attack rate predicted from evolutionary simulations. Shading represents the percentage (out of 10) of non-evolutionary simulations with the given attack rate and conversion efficiency where the predator and prey go extinct. In the lower left corner, the predator goes extinct and the prey persists. In

the upper right corner, the predator drives prey extinction. The ES attack rate is consistently below the predator-driven prey extinction threshold. Other parameters: d=1, m=2, and r=20.

Supplement 7: Effect of predator death rate on the evolutionary stable attack rate.

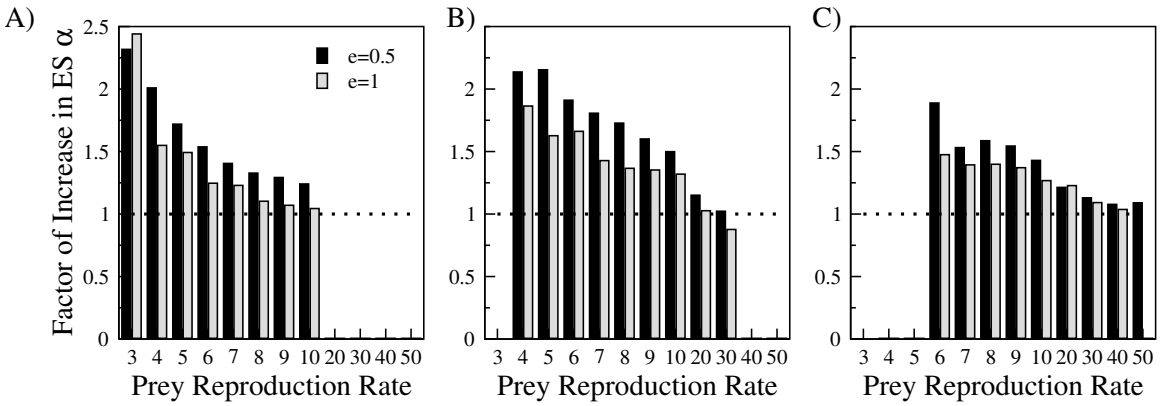

Figure S.2. Effect of predator death rate on the evolutionary stable attack rate. The factor of increase in the evolutionary stable attack rate (ES α) is shown for an increase in the predator death rate from (a) m=0.5 to m=1, (b) m=1 to m=2, and (c) m=2 to m=3 across prey reproduction rates. A factor of increase of 1 means the ES α did not change. The non-spatial model predicts a factor of increase of 1 (in other words, no evolutionary effect) for all prey reproduction rates and predator conversion efficiencies. When $d/m \geq 1$ (a), the increase in the ES attack rate tends to be larger for low prey reproduction rates but more quickly approaches no change. Other parameters: d=1, r=20.

Supplement 8: The effect of prey-to-predator conversion efficiency on "self-shading"

A predator's efficiency will impact an invader's *quasi-equilibrium* local density of prey as well as its *equilibrium* local density of prey (recall $\hat{q}_{N|P} = m/\alpha e$). The equilibrium local density of prey decreases with efficiency—a more efficient predator can have a positive growth rate at a lower local prey density. This effect alone predicts that efficiency decreases the intensity of self-shading (subtracting a smaller equilibrium density of prey from the quasi-equilibrium

density of prey for a given attack rate increases the invasion fitness). Thus, one would expect the ES attack rate to increase with efficiency. In fact, this is opposite to the predominant pattern shown in the main text (Fig. 2). However, the increased efficiency may decrease the quasi-equilibrium density of prey through the impact of the invader, by allowing it to co-opt more neighboring empty sites for its offspring, thereby suppressing local prey replenishment (there are fewer empty sites for prey offspring). This effect alone predicts that efficiency could increase the intensity of self-shading (subtracting the equilibrium density of prey for a given attack rate from a smaller quasi-equilibrium density of prey decreases the invasion fitness). Thus, one would expect the ES attack rate to decrease with efficiency, which agrees with the trends occurring in our simulations. Hence, overall, it appears that the effect of efficiency mediated by the quasi-equilibrium density of prey dominates over the effect of efficiency mediated by the equilibrium density of prey. However, the effect weakens with increasing prey reproduction—the slope of the log-log relationship between the ES attack rate and efficiency decreases with prey reproduction rate (see Fig. 5). This intuitively makes sense since the prey reproduction rate increases prey replenishment and therefore reduces the impact of efficiency on prey replenishment.

References

[1] Boots, M. & Sasaki, A. 1999 'Small worlds' and the evolution of virulence: infection occurs locally and at a distance. *Proc. R. Soc. B* **266**, 1933-1938.

[2] Pianka, E. 2000 Evolutionary Ecology. San Francisco: Benjamin Cummings.

[3] Yodzis, P. & Innes, S. 1992 Body size and consumer-resource dynamics. *Am. Nat.* **139**, 1151-1175.

[4] Cohen, J. E., Pimm, S. L., Yodzis, P., & Saldana, J. 1993 Body sizes of animal predators and animal prey in food webs. *J. Anim. Ecol.* **62**, 67-78.

[5] Pervez, A. & Omkar 2005 Functional responses of coccinellid predators: An illustration of a logistic approach. *J. Insect Sci.* **5**, 5.

[6] Gutierrez, A. P., Morgan, D. J., & Haven-Stein, D. E. 1971 The ecology of *Aphis craecivora Koch* and subterranean clover stunt virus. i. The phenology of aphid populations and the epidemiology of virus in pastures in south-east Australia. *J. App. Ecol.* **8**, 699-721.

[7] Wong, M. C. & Barbeau, M. A. 2006 Rock crab predation of juvenille sea scallops: the functional response and its implications for bottom culture. *Aquacult. Int.* **14**, 355-376.

[8] Ansell, A. D., Dao, J.-C., & Mason, J. 1991 Three european scallops: *Pecten maximus*, *Chlamys* (*aequipecten*) *opercularis* and *C.* (*chlamys*) *varia*. In *Scallops, biology, ecology and aquaculture* (ed. S. E. Shumway), pp. 715-751. Amsterdam: Elsevier.

[9] Diller, L. V., & Johnson, D. R. 1988 Food habits, consumption rates, and predation rates of western rattlesnakes and gopher snakes in southwestern Idaho. *Herpetologica* **44**, 228-233.